Methane fluxes to the atmosphere from deepwater hydrocarbon seeps in the northern Gulf of Mexico

Lei Hu,[1] Shari A. Yvon-Lewis,[1] John D. Kessler,[1] and Ian R. MacDonald[2]

Received 8 April 2011; revised 21 October 2011; accepted 9 November 2011; published 13 January 2012.

[1] Three deepwater hydrocarbon seep sites in the northern Gulf of Mexico that feature near-seafloor gas hydrates, MC118 (depth = 900 m), GC600 (depth = 1250 m) and GC185 (depth = 550 m), were investigated during the Remote Sensing and Sea-Truth Measurements of Methane Flux to the Atmosphere (HYFLUX) study in July 2009. Continuous measurements of air and sea surface concentrations of methane were made to obtain high spatial and temporal resolution of the diffusive net sea-to-air fluxes. The atmospheric methane fluctuated between 1.70 and 2.40 parts per million (ppm) during the entire cruise except for high concentrations (up to 4.01 ppm) sampled during the end of the occupation of GC600 and the transit between GC600 and GC185. In conjunction with air-mass back trajectory analysis, these high concentrations are likely from a localized methane source to the atmosphere. Methane concentrations in surface seawater and methane net sea-to-air fluxes show high temporal and spatial variability within and between sites. The presence of ethane and propane in the surface seawater indicates a thermogenic source in the plume areas, suggesting the surface methane could be at least partly attributable to transport from the deepwater hydrocarbon seeps. Results from interpolations within the survey areas show the daily methane fluxes to the atmosphere at the three sites range from 0.744 to 300 mol d^{-1}. Extrapolating the highest daily sea-to-air flux of methane to other deepwater seeps in the northern Gulf of Mexico suggests that the net diffusive sea-to-air flux from deepwater hydrocarbon seeps in this region is an insignificant source to the atmospheric methane.

Citation: Hu, L., S. A. Yvon-Lewis, J. D. Kessler, and I. R. MacDonald (2012), Methane fluxes to the atmosphere from deepwater hydrocarbon seeps in the northern Gulf of Mexico, *J. Geophys. Res.*, *117*, C01009, doi:10.1029/2011JC007208.

1. Introduction

[2] Methane (CH_4), one of the most important greenhouse gases, has a warming potential 23 times that of carbon dioxide over a 100 year time horizon [*Ramaswamy et al.*, 2001]. It is also actively involved in tropospheric ozone production and stratospheric ozone destruction. The total amount of methane reserved in the form of gas hydrate is about 2×10^6 Tg in a global inventory [*Boswell and Collett*, 2011]. It is comparable to about 400 times the total mass of the global atmospheric methane, 4850 ($\pm$242) Tg [*Intergovernmental Panel on Climate Change*, 2001]. Although the gas hydrate is an enormous methane reservoir, the contribution of the gas hydrate from the seafloor to the atmospheric methane budget is poorly characterized. It is estimated that marine seeps emit 18–48 Tg yr^{-1} of methane from the continental shelves to the overlying water column [*Hornafius et al.*, 1999]. However, the global emission from gas hydrates to the atmosphere is less than 5 Tg yr^{-1} [*Reeburgh*, 2007].

[3] Methane released from the seafloor or produced in microenvironments in the water column [e.g., *Cynar and Yayanos*, 1991; *de Angelis and Lee*, 1994] can reach the atmosphere through turbulent diffusion or rising bubbles. In shallow water, rising bubbles are the predominant pathway for delivering methane from seeps to the atmosphere, while the net sea-to-air fluxes via diffusion are also considerable [*Mau et al.*, 2007; *Schmale et al.*, 2005]. In deep water systems, turbulent diffusion is a commonly cited pathway to deliver methane to the atmosphere, whereas it is still debatable whether or not bubbles are capable of surviving from the seafloor to the surface and, if so, how much methane would be displaced by other gases (i.e., oxygen, nitrogen etc.) as they are stripped out of the water as the bubble moves to the surface [*McGinnis et al.*, 2006; *Rehder et al.*, 2002, 2009]. Methane transport via rising bubbles from the deepwater seeps to the atmosphere depends on a variety of geological and physical parameters, including intensity and composition of the seepages, bubble initial size, release depth, bubble path, and dissolution rate [*Leifer and MacDonald*, 2003]. Most previous studies reported that the diffusive net sea-to-air fluxes of methane from deepwater

[1]Department of Oceanography, Texas A&M University, College Station, Texas, USA.
[2]Earth Ocean Atmosphere Department, Florida State University, Tallahassee, Florida, USA.

0148-0227/12/2011JC007208

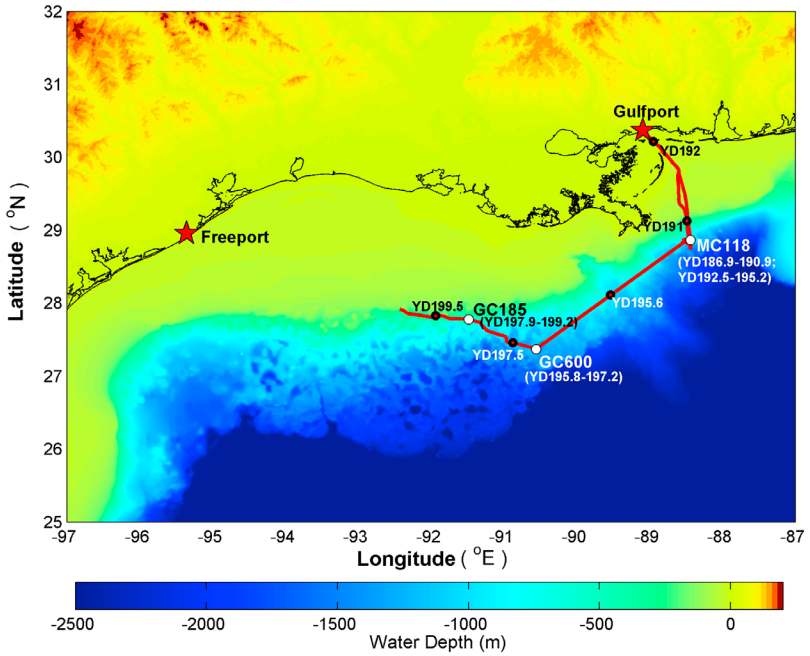

Figure 1. Cruise track (red line) of HYFLUX cruise in July 2009. Colored surface of the map indicates the water depths and land surface elevations. The bathymetric data are from the NOAA National Geophysical Data Center (http://www.ngdc.noaa.gov/mgg/bathymetry/relief.html). White circles denote the locations of the three seep sites; black circles mark the year days (YD) along the cruise track; red stars stand for the ports where the ship departed or arrived.

seep systems (water depth >200 m) are insignificant [e.g., *Kessler et al.*, 2006; *Reeburgh et al.*, 1991; *Schmale et al.*, 2005; *Yvon-Lewis et al.*, 2011]. However, one recent study suggests that the diffusive net sea-to-air flux of methane from the deepwater hydrocarbon seeps to the atmosphere could be considerable [*Solomon et al.*, 2009].

[4] To better understand and quantify the diffusive net sea-to-air fluxes of methane from deepwater hydrocarbon seeps, we investigated three deepwater seeps featuring near-seafloor gas hydrate in the northern Gulf of Mexico. High spatial and temporal resolution measurements were made to determine the net sea-to-air fluxes of methane over these hydrocarbon seeps.

2. Method

2.1. Location and Measurements

[5] The HYFLUX cruise took place in the northern Gulf of Mexico during July 2009 (4–19 July 2009) aboard the R/V *Brooks McCall*. Intensive surface surveys were conducted above three active seeps, MC118 (Rudyville, 28.8522°N, 88.4928°W, 900 meters below sea level (mbsl)), GC600 (Oil Mountain, 27.3652°N, 90.5642°W, 1250 mbsl), and GC185 (Bush Hill, 27.7823°N, 91.5080°W, 550 mbsl) (Figure 1), which were characterized by seafloor gas hydrate deposits that were partly exposed to seawater. Active oil and gas venting was confirmed by a remotely operated vehicle (ROV) at fixed locations within all three sampling sites. Air and surface seawater samples were analyzed continuously (except for brief maintenance intervals) during occupation of the sites and transits. The air-sea sampling plan had two modes: (1) a coarse regular grid, where samples were spaced at a kilometer scale and (2) a fine sampling scale that occurred as the ship loitered above the ROV, where samples were spaced ≤10 m. The ship speed was kept below 4 knots over most of the seep areas (Figure 2e).

[6] To measure the diffusive net sea-to-air fluxes of methane and infer its origin, atmospheric and surface seawater dissolved C_1-C_3 hydrocarbons were measured continuously with an automated sampling system coupled to a Weiss-type equilibrator and a Gas Chromatograph/Flame Ionization Detector (GC/FID, Agilent 6850) system. This technique only quantifies the diffusive net sea-to-air flux of dissolved methane and not the direct bubble injection of methane to the atmosphere; however, direct bubble injection to the atmosphere could be manifested in the data as enhanced atmospheric concentrations relative to surface seawater.

[7] Air samples were pumped continuously at ~6 L min^{-1} through 0.63 cm ID Synflex tubing (Motion Industries, Texas) mounted on the railing on the top of flying bridge and running to the laboratory. Surface seawater (about 4 m below the sea surface) was pumped into the Weiss-type equilibrator at 15 L min^{-1}. Equilibrator headspace and ambient air were alternately sampled every 6 min using a stream select valve. The sample stream passed through a 20 μL sampling loop after being dehumidified by a Nafion dryer (Permapure Inc). The Nafion dryer and the 20 μL sampling loop were flushed with the sample air at a rate of 25 mL min^{-1} for 90 seconds before injection into the GC/FID, which was equipped with a 15 m long, 32 μm ID GS-GasPro column (1 m precolumn and 14 m main column) with nitrogen carrier gas. Prior to the cruise, a series of standard mixtures (C_1-C_3) ranging from 0 to

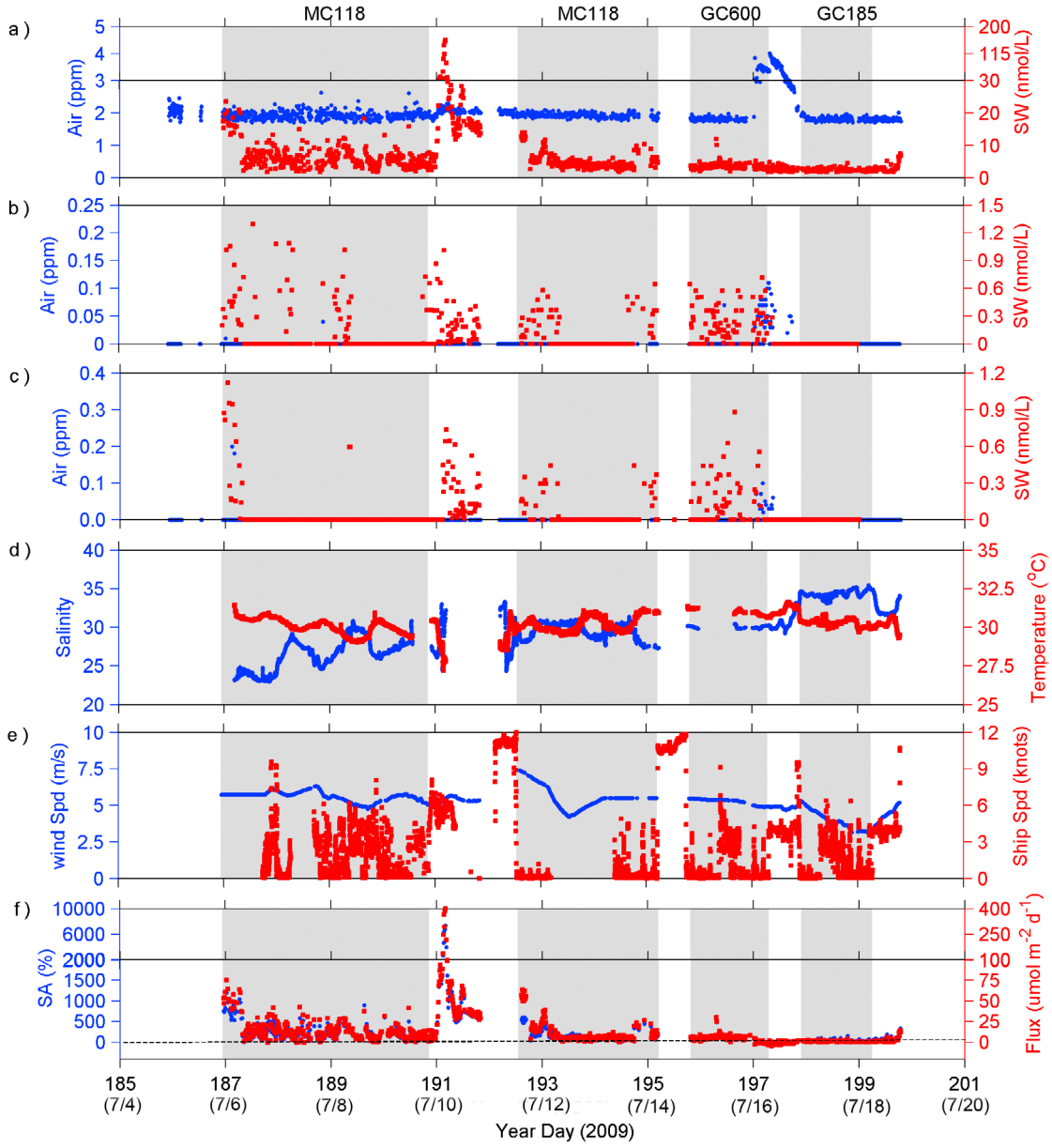

Figure 2. (a) Atmospheric mixing ratios (blue) and surface seawater concentrations (red) of methane; the scales for surface seawater methane in ranges of 0–30 and 30–200 nmol L^{-1} are different. Atmospheric mixing ratios (blue) and surface seawater concentrations (red) of (b) ethane and (c) propane. (d) Sea surface salinity (blue) and temperature (red) and (e) 24 hour averaged wind speeds at 10 m above sea level prior to sampling (blue) and ship speeds along the cruise track (red). (f) Saturation anomalies (blue) and net sea-to-air fluxes (red) of methane; different scales for saturation anomalies in ranges of −40–2000% and 2000–10,000% and fluxes in ranges of −20–100 and 100–400 μmol m^{-2} d^{-1}; dash line marks zero saturation anomaly and zero flux. Concentrations of zeros for Figures 2a–2c indicate concentrations below the instrument detection limit. Grey shadows mark the time periods over three seep sites. X-axis is the year day of 2009 and the corresponding month/day is labeled in the brackets.

1000 parts per million (ppm) were made using two known concentration standards (15 and 1000 ppm) from Scott Specialty Gases. Standards with methane concentrations at 0.09 (±0.01), 1.09 (±0.02), 1.69 (±0.02) and 2.88 (±0.06) ppm were also calibrated against a whole air tank, which was calibrated to the NOAA-04 methane scale. The standards with methane concentrations at 0.09–2.88 ppm were used to create a standard curve to calibrate the instrument. Higher concentration standards 15 (±1.5), 503 (±25) and 1000 (±50) ppm were also run and used as an alternate calibration curve when the measured concentration exceeded the lower calibration range. The precision of the system was determined from five standard injections. The precision for concentrations ≤3 ppm was 3% for methane, 2% for ethane and

3% for propane. The precision for concentrations >3 ppm was less than 1% for methane, ethane and propane.

[8] The sea surface temperature and salinity were continuously measured by a conductivity-temperature-depth (CTD) sensor from Sea-Bird Electronics (SBE 19 plus) at the outflow of the equilibrator. Wind speeds and directions were continuously measured by an anemometer at a height of ~9 m above the sea level.

2.2. Equilibrator Concentration Correction

[9] The equilibrator headspace technique has been used for the determination of the net sea-to-air fluxes of many dissolved gases including but not limited to halocarbons [*Butler et al.*, 2007 and references therein; *Hu et al.*, 2010 and references therein], CO_2 [*Takahashi et al.*, 2009 and references therein] and methane [*Amouroux et al.*, 2002; *Bange et al.*, 1994, 1996, 1998; *Kourtidis et al.*, 2006; *Rhee et al.*, 2009] over the past 20 years.

[10] Due to the different solubilities for different gases, the time needed for the trace gas concentration in the headspace to reach equilibrium with the incoming seawater is different for each trace gas. The headspace mass concentration, C_e, at a time, t, can be expressed with the following equation when the equilibrator vent flow, Q_v, is zero [*Johnson*, 1999]:

$$C_e = \left(C_i - \frac{C_w}{\alpha}\right)e^{-(t/\tau_1)} + \frac{C_w}{\alpha}, \tag{1}$$

where $\tau_1 = \frac{v_e}{Q_w \varepsilon \alpha}$; V_e is the volume of the headspace, 12.5 L; Q_w is the volumetric flow rate of the seawater, 15 L min^{-1}; ε is a dimensionless equilibrator coefficient, which is typically about 0.3–0.4 [*Johnson*, 1999]; α is the Oswald solubility coefficient; C_i is the initial mass concentration in the headspace and C_w is the mass concentration of the trace gas in the incoming seawater.

[11] When the equilibrator vent flow, Q_v, is not zero, the air in the headspace is removed and replaced by the ambient air at a rate of Q_v. The trace gas concentration in the headspace can then be expressed by the following equation [*Johnson*, 1999]:

$$C_e = \frac{\frac{C_w}{\alpha\tau_1}\left(1 - e^{-t/\tau_2}\right) + \frac{C_a}{\tau_v}\left(1 - e^{-t/\tau_2}\right) + \frac{C_i}{\tau_2}e^{-t/\tau_2}}{1/\tau_2}, \tag{2}$$

where $\tau_v = \frac{v_e}{Q_v}$ and $\frac{1}{\tau_2} = \frac{1}{\tau_1} + \frac{1}{\tau_v}$; C_a is the mass concentration of the trace gas in the ambient air.

[12] Under normal operating conditions, the equilibrator vent flow is zero except the duration when the instrument is flushing the dryer and sample loop (i.e., collecting the headspace air sample). Assuming the equilibrator vent flow is off for a period of t_1 (min) and on for a period of t_2 (min) at a rate of Q_v (ml min^{-1}), the trace gas concentration in the headspace at $t_1 + t_2$ can be expressed as

$$C_e = \frac{\frac{C_w}{\alpha\tau_1}\left(1 - e^{-t_2/\tau_2}\right) + \frac{C_a}{\tau_v}\left(1 - e^{-t_2/\tau_2}\right)}{1/\tau_2} + \left(\left(C_i - \frac{C_w}{\alpha}\right)e^{-t_1/\tau_1} + \frac{C_w}{\alpha}\right)e^{-t_2/\tau_2}. \tag{3}$$

Since the trace gas concentrations in the ambient air and in the equilibrator headspace were measured, C_a, C_i, and C_e are known. The trace gas concentration in seawater can be expressed as a function of C_a, C_i, and C_e (equation (4))

$$C_w = \frac{C_e - \frac{\tau_2}{\tau_v}\left(1 - e^{-t_2/\tau_2}\right)C_a - e^{-\left(\frac{t_1}{\tau_1} + \frac{t_2}{\tau_2}\right)}C_i}{\frac{\tau_2\left(1 - e^{-t_2/\tau_2}\right)}{\alpha\tau_1} + \frac{\left(1 - e^{-t_1/\tau_1}\right)e^{-t_2/\tau_2}}{\alpha}}. \tag{4}$$

In this study, the vent flow, 25 ml min^{-1}, was only on for 2.5 min between two seawater measurements, resulting in only 1% of difference in the C_w compared to the case without the vent flow. Given such a small effect, we can simplify equation (4) by assuming the vent flow is 0 during t_1 to t_2. Then τ_v is equal to 0, and τ_1 is equal to τ_2. Equation (4) can be expressed as

$$C_w = \frac{C_e - C_i e^{-\left(\frac{t_1 - t_2}{\tau_1}\right)}}{\frac{1 - e^{-\left(\frac{t_1 + t_2}{\tau_1}\right)}}{\alpha}}. \tag{5}$$

In equations (1)–(5), it is assumed that the trace gas concentration in the seawater is constant during t_1 and t_2. However, in reality, this assumption may not be true especially when the ship speed is fast. Therefore, assuming the seawater concentration is constant during a very short time period (Δt) (i.e., <1 s) and the seawater concentrations are $C_{w_1}, C_{w_2}, \ldots, C_{w_{n-1}}, C_{w_n}$ for each Δt ($n\Delta t = t_1 + t_2$), the trace gas concentration in the headspace can be expressed by

$$C_e = \left(C_i - \frac{C_{w_1}}{\alpha}\right)e^{-\frac{n\Delta t}{\tau_1}} + \left(\frac{C_{w_1} - C_{w_2}}{\alpha}\right)e^{-\frac{(n-1)\Delta t}{\tau_1}} + \left(\frac{C_{w_2} - C_{w_3}}{\alpha}\right)e^{-\frac{(n-2)\Delta t}{\tau_1}} + \ldots + \left(\frac{C_{w_{n-1}} - C_{w_n}}{\alpha}\right)e^{-\frac{\Delta t}{\tau_1}} + \frac{C_{w_n}}{\alpha}. \tag{6}$$

By substituting the C_e in equation (5) with equation (6), C_w can be expressed by

$$C_w = \frac{1 - e^{-\Delta t/\tau_1}}{1 - e^{-n\Delta t/\tau_1}}\left(C_{w_1}e^{-\frac{n-1}{\tau_1}\Delta t} + C_{w_2}e^{-\frac{n-2}{\tau_1}\Delta t} + C_{w_3}e^{-\frac{n-3}{\tau_1}\Delta t} + \ldots + C_{w_{n-1}}e^{-\frac{1}{\tau_1}\Delta t} + C_{w_n}\right). \tag{7}$$

Assuming $a_i = \frac{1 - e^{-\Delta t/\tau_1}}{1 - e^{-n\Delta t/\tau_1}}e^{-\frac{n-i}{\tau_1}\Delta t}$ (i = 1, 2, 3, …, n), C_w can be rewritten as

$$C_w = a_1C_{w_1} + a_2C_{w_2} + a_3C_{w_3} + \ldots + a_{n-1}C_{w_{n-1}} + a_nC_{w_n}. \tag{8}$$

Therefore, the fractional contributions of the true seawater concentrations, $C_{w_1}, C_{w_2}, \ldots, C_{w_{n-1}}, C_{w_n}$, to the corrected seawater concentration (C_w) are $a_1, a_2, \ldots, a_{n-1}, a_n$. For the very soluble gases (i.e., CO_2, N_2O), $a_1, a_2, \ldots, a_{n-1}, a_n$ exponentially increase from 0 to 1 as a_1 goes to a_n, and C_w is more representative of an instantaneous incoming seawater concentration. For the less soluble gases (i.e., CH_4, CO), $a_1, a_2, \ldots, a_{n-1}, a_n$ are close to $1/n$ and C_w is more representative of an average seawater concentration during the last $n\Delta t$ min. In this study, the seawater concentrations were calculated using equation (4), and they represent average seawater concentrations over a period of 12 min. As the ship speed

Table 1. Mean Atmospheric Methane Mixing Ratios, Seawater Methane Concentrations, Saturation Anomalies and Net Sea-to-Air Fluxes of Methane at the Three Seep Sites[a]

Sites	Atmospheric CH_4 Mixing Ratio (ppm)	Seawater CH_4 Concentration (nmol L^{-1})	Saturation Anomaly (%)	Averaged Wind Speed (m s^{-1})	Flux (μmol m^{-2} d^{-1})	
					W92[b]	S07[c]
MC118	1.93 (1.71–2.62)	5.85 (1.76–23.5)	207 (−6.42–1196)	5.6	15.4 (−0.52–86.1)	12.8 (−0.45–75.0)
GC600	2.13 (1.72–3.83)	3.61 (1.76–11.9)	90.5 (−46.0–598)	5.3	5.41 (−4.19–34.9)	4.67 (−3.65–30.4)
GC185	1.81 (1.71–1.98)	2.41 (1.72–4.48)	39.6 (2.33–156)	4.0	1.25 (0.08–4.13)	1.07 (0.07–3.60)

[a]Ranges of values are given in parentheses.
[b]W92 refers to the flux calculated using the *Wanninkhof* [1992] gas transfer velocity parameterization.
[c]S07 refers to the flux calculated using the *Sweeney et al.* [2007] gas transfer velocity parameterization.

was in a range of 0–4 knots when sampling, 12 min represents a distance of 0–1480 m.

2.3. Net Sea-to-Air Flux Calculation

[13] The net sea-to-air flux (F) is calculated by

$$F = k_w(C_w - \alpha C_a), \tag{9}$$

where k_w is the gas transfer velocity (m d^{-1}) [*Sweeney et al.*, 2007], and C_w, C_a and α are defined above. The gas transfer velocity parameterization from *Sweeney et al.* [2007] is an improvement over the typical *Wanninkhof* [1992] parameterization since they closed the previous gap between field measurements [*Liss and Merlivat*, 1986; *Nightingale et al.*, 2000] and radiocarbon estimates [*Tans et al.*, 1990; *Wanninkhof*, 1992] on this parameter.

[14] The gas transfer velocity (k_w) from *Sweeney et al.* [2007] is expressed as

$$k_w = 0.27u_{10}^2\left(\frac{Sc}{660}\right)^{-0.5}, \tag{10}$$

where Sc is the Schmidt Number of methane in seawater from *Wanninkhof* [1992] and u_{10} is the 10 m normalized wind speed (m s^{-1}) determined using the equation given by *Large and Pond* [1982].

3. Results

[15] Atmospheric methane during this cruise ranged from 1.70 to 4.01 ppm with a mean of 2.03 ppm (Figure 2a). The atmospheric methane fluctuated around a background concentration of 1.92 ppm during the occupation of the sites and transits except at the end of GC600 and the transit to GC185 (Figure 2a). The surface seawater methane concentrations ranged from 1.76 to 23.5 nmol L^{-1} at MC118, 1.76 to 11.9 nmol L^{-1} at GC600, and 1.72 to 4.48 nmol L^{-1} at GC185 (Table 1). The presence of ethane (Figure 2b) and propane (Figure 2c) in the surface seawater over the seep area (mainly at MC118 and GC 600) indicates a thermogenic contribution from the deepwater hydrocarbon seeps. The maximum methane concentration observed in surface seawater during this study, 156 nmol L^{-1}, was observed on year day (YD) 191 (10 July 2009) on the continental shelf offshore from Louisiana (Figures 1 and 2a). The corresponding atmospheric methane concentrations reached 2.10 ppm due to the net sea-to-air flux (Figure 2a). Increased ethane and propane along with elevated salinity and decreased temperature (Figures 2b–2d) suggest that the elevated methane in the surface seawater may be associated with upwelling of hydrocarbon enriched waters. A similar feature in the surface seawater was observed in the same region in June 2010 during the Persistent Localized Underwater Methane Emission Study (PLUMES) [*Yvon-Lewis et al.*, 2011].

[16] The methane saturation anomaly is defined as the percent difference between the partial pressures of methane in surface seawater and air. They ranged from −51.8% to 7.43×10^3% (Figure 2f). The calculated net sea-to-air fluxes ranged from −4.68 to 416 μmol m^{-2} d^{-1} (Figure 2f). The mean net sea-to-air flux at each of the three seep areas was 12.8 (MC118), 4.67 (GC600) and 1.07 μmol m^{-2} d^{-1} (GC185) (Table 1). To compare the results from this study to those from previous studies, we calculated the flux using the gas transfer velocity from *Wanninkhof* [1992] in addition to using the *Sweeney et al.* [2007] relationship described earlier. The calculated net sea-to-air methane fluxes from the deepwater hydrocarbon plume areas are 1–2 orders of magnitude lower than those from shallow water seep plume areas (Table 2) [*Mau et al.*, 2007; *Schmale et al.*, 2005]. For the deep water environment, the calculated fluxes from this study are in the same range as those determined from most previous studies (Table 2) [*Reeburgh et al.*, 1991; *Schmale et al.*, 2005; *Yoshida et al.*, 2004; *Yvon-Lewis et al.*, 2011]. However, they are three orders of magnitude lower than those reported by *Solomon et al.* [2009] who investigated the same region as the current study including one of the same identified seep sites.

4. Discussion

[17] Based on the results above, four main issues will be addressed in the following discussion: (1) the source for the elevated atmospheric methane during the transit from GC600 to GC185; (2) the diffusive net sea-to-air fluxes of methane over three seep sites and the extrapolated total fluxes of methane over the deepwater seep area in the northern Gulf of Mexico; (3) potential causes for the large discrepancy between the results from this study and those reported by *Solomon et al.* [2009]; and (4) the impact of small areas of high methane concentration hotspots on our regional air-sea flux estimate if extremely high concentrations existed in the surface seawater over a deepwater hydrocarbon plume area and were missed in this study.

4.1. Elevated Atmospheric Methane

[18] An area of elevated atmospheric methane with a maximum concentration of 4.01 ppm was observed on YD 197 (16 July) at GC600 (Figure 2a). The elevated atmospheric methane persisted for 19 h and extended over 50 km to the northwest of GC600 during the transit to GC185

Table 2. Diffusive Net Sea-to-Air Fluxes of Methane From Different Marine Environments

Location	Water Depth (m)	Flux[a] (μmol m^{-2} d^{-1})	Reference
	Deep Water Environments (>200 m)		
Deepwater hydrocarbon plume area in the northern Gulf of Mexico	550–1250	−4.19–86.1	this study
Deepwater hydrocarbon plume area in the northern Gulf of Mexico	500–600	200–10,500	*Solomon et al.* [2009]
Plume area during the Deepwater Horizon oil spill	1500	−0.055–1.83	*Yvon-Lewis et al.* [2011]
Sorokin Trough and Dnepr Area in Black Sea	>200	40.6–49.2	*Schmale et al.* [2005]
Central Black Sea	>200	27	*Reeburgh et al.* [2006]
Sea of Okhotsk	>200	0.36–88	*Yoshida et al.* [2004]
Baltic and North Seas	>200	−6.6–13.89	*Bange et al.* [1994]
Aegean Sea	>200	1.81	*Bange et al.* [1996]
Northwestern Levantine Basin	>200	3.02	*Bange et al.* [1996]
Open Ocean in the Atlantic	>200	0.3	*Rhee et al.* [2009]
Open Ocean in the Pacific	>1000	0.9–3.5	*Tilbrook and Karl* [1995]
	Shallow Water Environments (≤200 m)		
Coal Oil Point	<70	195	*Mau et al.* [2007]
Northwest Black Sea	<200	53	*Amouroux et al.* [2002]
Northwestern continental shelf of the Sea of Okhotsk	<200	0.47–11	*Yoshida et al.* [2004]
Shelf waters of Dnepr Area	<200	67	*Schmale et al.* [2005]
Coastal region of the Atlantic	<200	3.2	*Rhee et al.* [2009]

[a]Fluxes were calculated using the gas transfer velocity parameterization of *Wanninkhof* [1992].

(Figure 2a). Coincident elevated ethane and propane in the atmosphere suggest a thermogenic gas contribution (Figures 2b and 2c). The 24 h air-mass back-trajectories obtained from the NOAA Air Resources Laboratory (http://ready.arl.noaa.gov/HYSPLIT_traj.php) show that the air masses with increased atmospheric methane came from the same region as those with background concentrations of 1.81 ppm (Figure 3), suggesting a localized source rather than long-range transport. Since the methane concentrations in the underlying seawater were close to a seawater background concentration of 2.40 nmol L^{-1} (Figure 2a), methane transport via diffusive sea-to-air gas exchange is not the source of these high atmospheric concentrations.

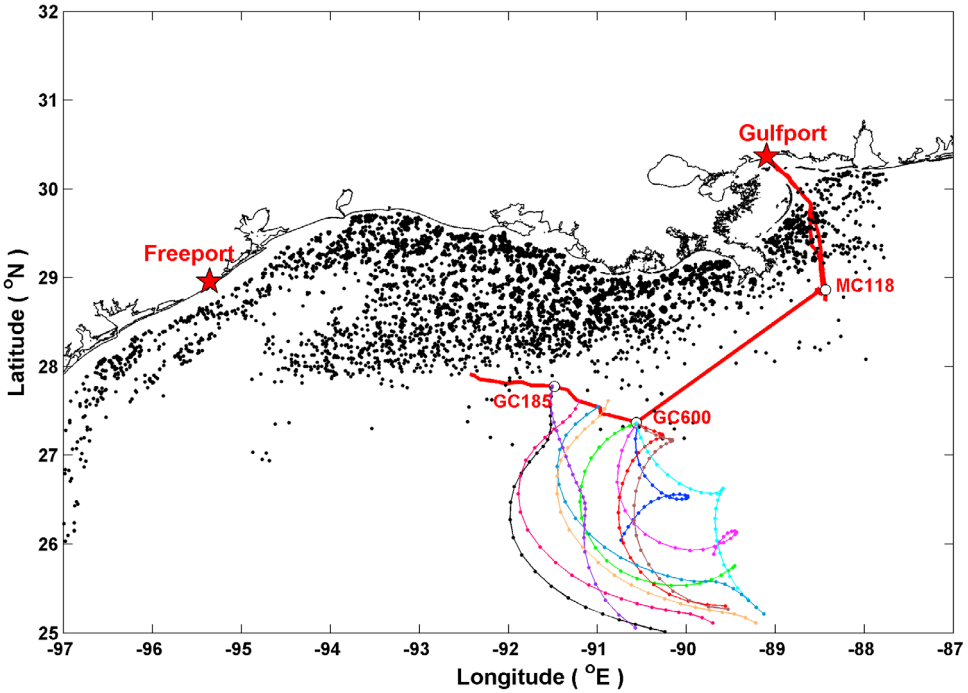

Figure 3. The 24 h back-trajectories of air masses (dot lines) and locations of oil platforms (black dots) in the northern Gulf of Mexico. Back-trajectories were downloaded from NOAA Air Resources Laboratory (http://ready.arl.noaa.gov/HYSPLIT_traj.php) and platform locations are from MMS Gulf of Mexico regional database (http://www.gomr.mms.gov/homepg/pubinfo/repcat/arcinfo/index.html). White circles denote the locations of three seep sites. Red stars stand for the ports where the ship departed or arrived.

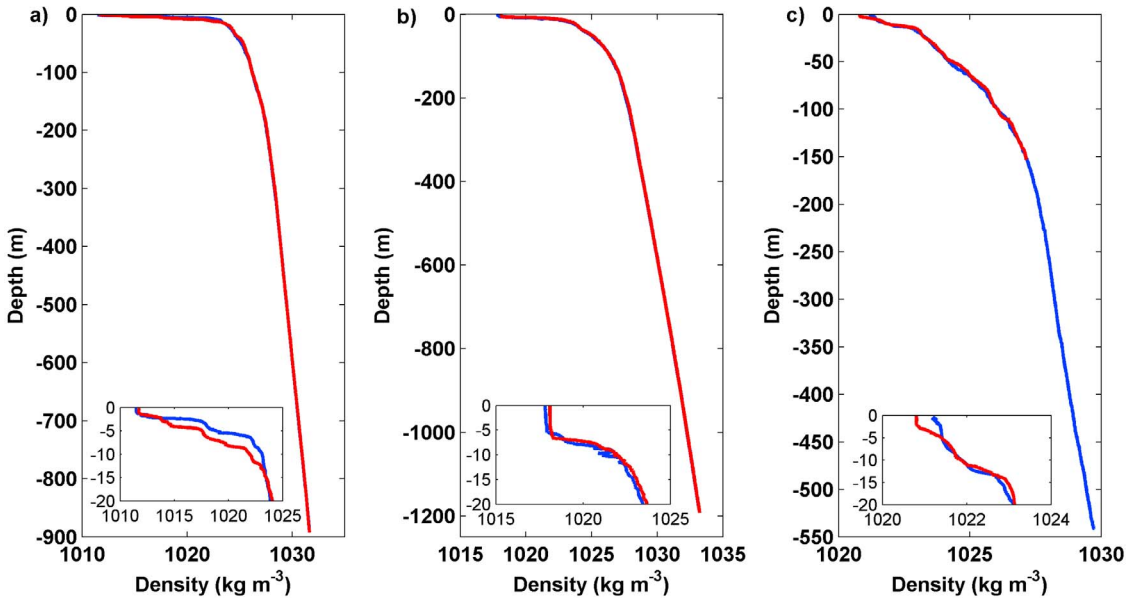

Figure 4. Vertical profiles of density at (a) MC118, (b) GC600 and (c) GC185. Red and blue lines stand for two randomly selected CTD casts from each site.

[19] Although bubbles traveling over 1000 m from a deepwater seep site have been observed [*Greinert et al.*, 2006], whether or not they can reach the surface is still debated [*McGinnis et al.*, 2006; *Rehder et al.*, 2009]. In this study, to increase the atmospheric methane concentration to 4.01 ppm (3.25 ppm averaged over the area with elevated methane concentrations), there would need to be 3×10^5 mol d^{-1} of methane released to the atmosphere assuming a marine boundary layer height of 700 m (data from http://ready.arl.noaa.gov/READYamet.php) and assuming that the elevated methane only spread out in a circle 100 m in diameter centered on the ship as it moved along the cruise track. It is not likely for direct methane transport via gas bubbles at GC600 to contribute such a large amount of methane to the atmosphere due to the strong pycnocline during the summer (Figure 4) and the 1200 m water depth at this site. While slicks were observed from the ship at this site along with intermittent oil droplets rising to the surface, surface water concentrations were 2.85 ± 0.73 (1σ) nmol L^{-1}, suggesting that these droplets were not carrying high concentrations of methane. Since the observation of the elevated atmospheric methane to the northwest of GC600 does coincide with satellite data from 20 July showing very extensive oil slicks over this broad region of the Gulf, we could not completely exclude the possibility that methane could be transported inside of the oily bubbles to the atmosphere. However, we cannot provide an appropriate mechanism for this possibility.

[20] Fugitive release to the atmosphere directly from oil platforms around GC600 is possible (Figure 3). Given the fact that no significantly elevated atmospheric methane concentrations were observed near the recovery ships during the Deepwater Horizon oil spill, which were flaring tremendous amounts of gas [*Yvon-Lewis et al.*, 2011], flaring itself is an unlikely source of methane to the atmosphere. Not flaring or accidentally releasing gas from the drilling oil platform during this time is not likely to be the explanation either based on the drilling records from the Drilling Rig OCEAN MONARCH (the rig close to GC600). A likely explanation could be an undetected leak from one or more of the nearby oil platforms.

4.2. Methane Net Sea-to-Air Fluxes Over the Seep Area in the Northern Gulf of Mexico

[21] High spatial variability was observed in sea surface methane and net sea-to-air fluxes over the three seep areas (Figures 5 and 6). Overall, MC118 had higher sea surface methane concentrations and higher net sea-to-air fluxes than either GC600 or GC185 (Tables 1 and 3 and Figures 5 and 6). GC600 is the oiliest site surveyed during this study. Although surfactants can inhibit bubble dissolution and enhance the methane transport, lower surface seawater methane concentrations and lower diffusive fluxes were observed than those at MC118. GC185 is the shallowest site occupied during this study. During a prior study at this site, a methane concentration of 608 nmol L^{-1} at a water depth of ~20 m was reported and used to determine a net sea-to-air flux of 3420 μmol m^{-2} d^{-1} in the plume area [*Solomon et al.*, 2009]. Therefore, higher methane concentrations in the air and sea surface as well as higher fluxes were anticipated. However, both the atmospheric methane and the sea surface (4 mbsl) methane were near background (Table 1). Spatial variability between sites is associated with characteristics of their geological and physical environment, e.g., seep intensity, oil-water ratio, water depth, currents, and mixed layer depth. Spatial variability within one seep site (Figure 5) is related with the rising angle of the bubbles and the directions of mid-depth and surface currents. High temporal variability within one seep site was also observed during our surface survey (Figures 2 and 6). The magnitudes of the fluxes and the elevated flux areal extent vary from day to day (Table 3 and Figure 6). The temporal variability of

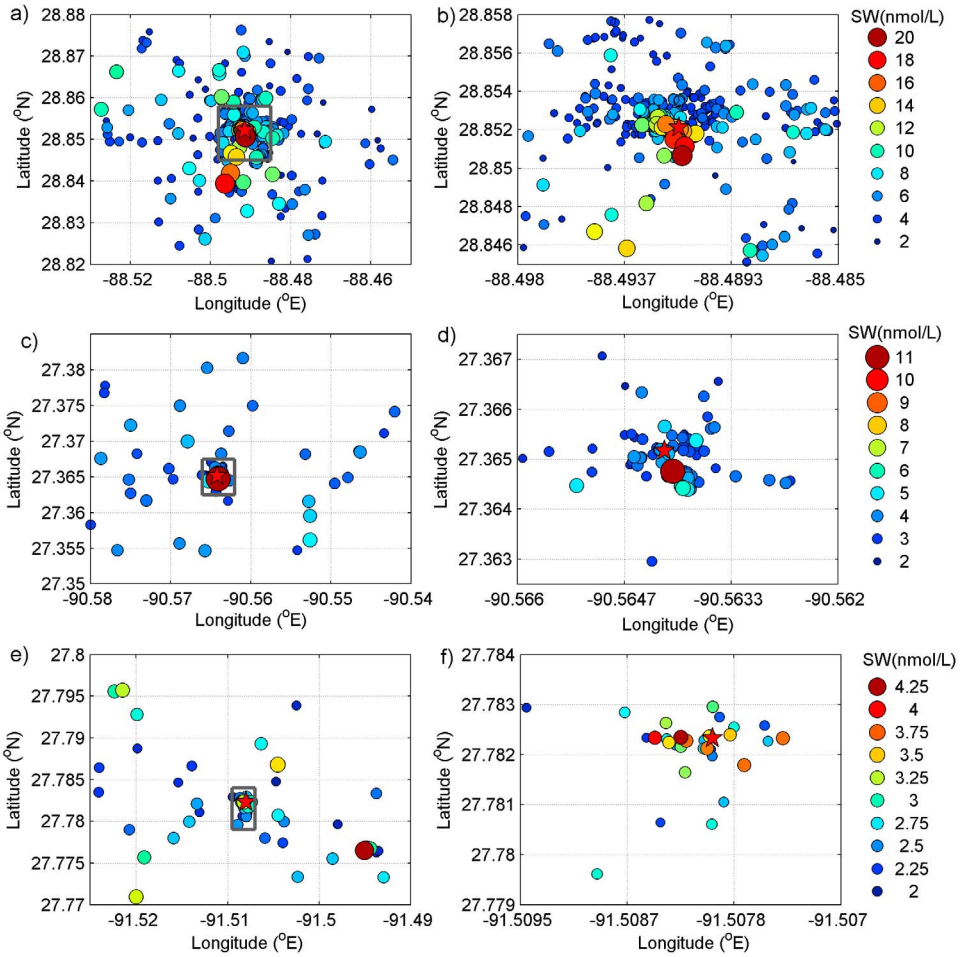

Figure 5. Methane concentrations in surface seawater at (a and b) MC118, (c and d) GC600 and (e and f) GC185. Grey rectangles in Figures 5a, 5c and 5e indicate the blown-up regions, which are plotted in Figures 5b, 5d and 5f. Red stars indicate the locations of the seeps.

methane fluxes could be due to changes in seepage rates, currents, wind speeds, surface wave action, etc. [*Clark et al.*, 2003, 2010; *Greinert et al.*, 2006; *Leifer and Boles*, 2005; *Leifer et al.*, 2006; *Quigley et al.*, 1999].

[22] The daily methane mass flux distribution for each survey area was determined by interpolation using natural neighbor, inverse distance weighted interpolation, and kriging (Table 3). The three different interpolation methods do not produce significantly different fluxes. Since the natural neighbor method produced a smoother shape, we chose this algorithm as our main interpolation method for plotting the mass flux distribution over the seep sites. Due to the high temporal and spatial variability of the methane fluxes within and between sites, it is difficult to extrapolate the observed net sea-to-air fluxes to other periods or to other hydrocarbon seeps (Figures 5 and 6). However, we can approximate the upper limit of the diffusive net sea-to-air flux of methane from the deepwater hydrocarbon seeps in the northern Gulf of Mexico under normal conditions (i.e., no mud volcanoes or submarine earthquake) by assigning the highest daily flux determined in this study, 300 mol d^{-1} (per seep site), to other deepwater hydrocarbon seeps in this region. Large uncertainty exists in the number of active seeps in the northern Gulf of Mexico. Geophysical anomalies generated by seeps in the geologic past exceed 5000 possible sites [*Frye*, 2008] whereas preliminary results for seeps detected by remote sensing (see the detailed method by *Garcia-Pineda et al.* [2010]) suggest a maximum number of active vents about 1500. Assuming that each of the 1500–5000 seeps in the northern Gulf of Mexico has daily net sea-to-air flux of 300 mol d^{-1} and they persistently emit methane to the atmosphere at the same rate over a one-year period, the total diffusive net sea-to-air flux from deepwater hydrocarbon seeps in the northern Gulf of Mexico is about 3–9 Gg yr^{-1}. Compared with the total annual emission of methane to the atmosphere, 5.8×10^5 Gg yr^{-1} [*Denman et al.*, 2007], the contribution of the net diffusive sea-to-air flux from deepwater hydrocarbon seeps in the northern Gulf of Mexico is insignificant to the atmospheric methane budget.

4.3. Explanation for Flux Discrepancy

[23] The three orders of magnitude methane flux discrepancy between this study and that reported by *Solomon et al.* [2009] is mainly attributable to the surface seawater methane values used in the flux equation (equation (9)). The "surface" seawater methane concentrations reported by *Solomon et al.* [2009] were in the range of 57.1–1609 nmol L^{-1} while

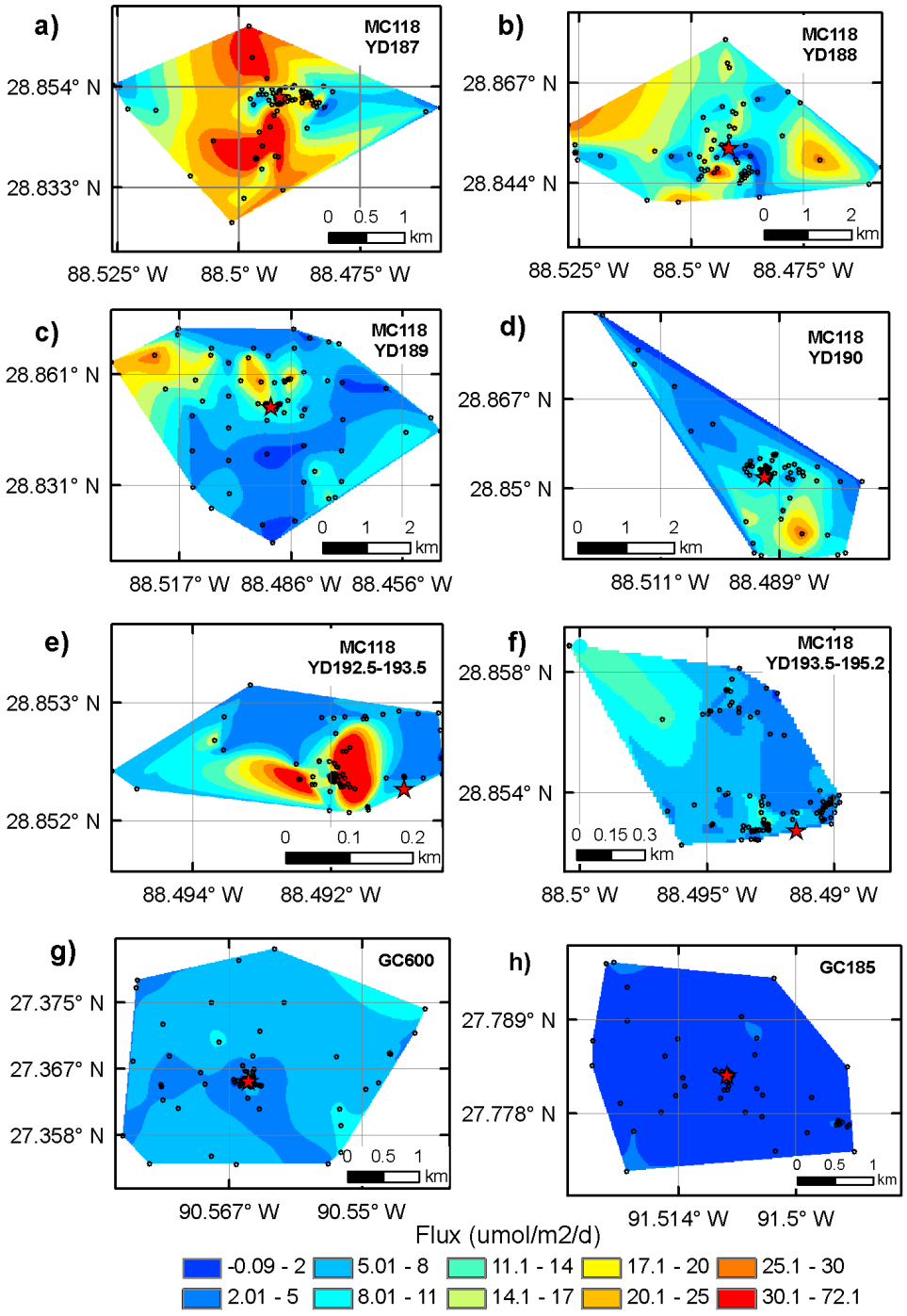

Figure 6. Contour plots of methane net sea-to-air fluxes at the three seep sites using natural neighbor. Red stars indicate the locations of the seeps. Black circles stand for the locations of the flux measurements.

the methane concentrations in this study ranged from 1.72 to 23.5 nmol L^{-1}. Although we cannot exclude the possibility of temporal variability, we can evaluate the methodological differences between these two studies. How each study defines a surface sampling depth is a key factor that bears consideration. In the present study, seawater was continuously sampled from ~4 m water depth within the mixed layer as the ship was moving. Mean mixed layer depths were 4.8 m (0–28.8 m; median: 3.5 m; 32 CTD casts) at MC118, 4.9 m (4.2–5.5 m; 2 CTD casts) at GC 600, and 2.1 m (1.4–2.6 m; 3 CTD casts) at GC185 (Figure 4). When determining the air-sea flux using the air-sea concentration gradient, the dissolved concentrations must be measured as close to the surface as possible. By contrast, the shallowest sample collected by *Solomon et al.* [2009] was around 20 m. Their temperature and salinity profiles (see supplementary materials of *Solomon et al.* [2009]) do not display a mixed layer depth below 20 m. Therefore, the surface water value they used to calculate methane fluxes were not diagnostic of true surface water values.

Table 3. Mass Fluxes Over the Survey Area Using Different Interpolation Gridding Methods[a]

			Natural Neighbor		Inverse Distance Weighted		Kriging	
Sites	Survey Area (km^2)	Area With Fluxes $\geq$8 μmol m^{-2} d^{-1} (km^2)	Area Weighted Mean Flux (μmol m^{-2} d^{-1})	Mass Flux (mol d^{-1})	Area Weighted Mean Flux (μmol m^{-2} d^{-1})	Mass Flux (mol d^{-1})	Area Weighted Mean Flux (μmol m^{-2} d^{-1})	Mass Flux (mol d^{-1})
MC118								
YD 187	15.15	14.00	19.8	300	21.5	326	23.2	352
YD 188	16.27	13.91	13.2	215	12.0	195	11.3	183
YD 189	34.64	12.31	7.82	271	8.68	301	9.11	316
YD 190	8.530	3.430	7.75	66.1	8.70	74.2	8.82	75.2
YD 192.5–193.5	0.06155	0.03014	12.1	0.744	15.5	0.954	18.7	1.15
YD 193.5–195.2	0.5318	0.0055	6.98	3.71	6.36	3.38	6.23	3.31
GC600	8.571	0.407	6.05	51.9	5.53	47.4	5.26	45.1
GC185	6.686	0.000	1.02	6.85	1.03	6.86	1.00	6.69

[a]The boundaries for the gridded fluxes are shown in Figure 6.

[24] A contributing but minor factor to the differences in net sea-to-air fluxes reported in the two studies involves the atmospheric methane concentrations used in the flux calculation. *Solomon et al.* [2009] used an averaged atmospheric methane concentration for their flux calculations, while the atmospheric mixing ratios were measured once every 12 min locally during the current study. Atmospheric methane ranged from 1.70 to 4.01 ppm over the seep sites during the current study. At times, the atmospheric methane concentrations were over twice the average background concentration. In some places during the occupation of GC600, the surface ocean acted as a sink for atmospheric methane and would have been misinterpreted as a source to the atmosphere if average atmospheric methane concentrations were used in the flux calculations. Fluxes of methane from the ocean to the atmosphere or other incidental hydrocarbon emissions could result in perturbations to the local atmospheric methane concentrations, and these perturbations should be accounted for in the calculation of the flux.

4.4. Impact of Small Area High Concentration Hotspots on the Regional Air-Sea Flux

[25] To determine if the regional air-sea flux results from continuous air-sea measurements are more representative than discrete measurements, we investigate whether the technique used in this study could have missed a high methane concentration hotspot that is large enough to impact the overall flux from the plume area. To address this possibility, the sensitivity of the corrected seawater concentration (C_w) to the size and concentration of a potential hotspot is determined using equation (7). We assumed (1) that any corrected seawater concentration $\geq$4 nmol L^{-1} (twice the background concentration) indicated an observable hotspot and (2) that the ship left a background concentration of 2 nmol L^{-1} and immediately crossed a methane hotspot with a concentration ranging from 4 to 1609 nmol L^{-1} (the highest 20 m value reported by *Solomon et al.* [2009]). Under these conditions, a surface hotspot with a concentration of 1609 nmol L^{-1} is observable for a hotspot with a diameter $\geq$2 m when the ship speed is 4 knots (e.g., when the ship is conducting coarse surveys) (Figures 7a and 7c), and a diameter $\geq$5 cm when the ship speed is 0.1 knots (e.g., when the ship was holding a station) (Figures 7b and 7d). As the concentration of the hotspot decreases, the hotspot size required for unequivocal detection would exponentially increase (Figure 7).

[26] Since the corrected seawater concentration (C_w) is close to an average concentration over 12 min (see equation (7)), it averages out the high and low seawater concentrations. Here, we will assess the possible impact of missed hotspots along the survey track. Assuming the three seep sites only contain hotspots with methane concentrations of 1609 nmol L^{-1} and waters with background concentrations of 2 nmol L^{-1}, the possible sizes of the missed hotspots can be determined by equation (7) using the actual ship speeds and the observed concentrations. The area of each possible missed hotspot ranges from 5.2×10^{-4} m^2 to 77 m^2 and the total area of missed hotpots in each of the three plume areas is 181–930 m^2 (MC118), 51 m^2 (GC600) and 20 m^2 (GC185), corresponding to fluxes of 0.80–5.16 mol d^{-1} (MC118), 0.24 mol d^{-1} (GC600) and 0.05 mol d^{-1} (GC185) (Table 4). The mean flux over each plume area resulting from hotspots that might have been missed using the current survey technique accounts for only 1.7% (MC118), 0.5% (GC600) and 0.7% (GC185) of the integrated regional flux (Table 4).

[27] Another potential limitation of the survey technique used in this study is the possibility that hotspots between the survey tracks were never sampled. Since the extremely high surface water methane concentrations reported by *Solomon et al.* [2009] were from GC185, we use this site to investigate the impact of missed hotspots between the survey tracks. Assuming that either the missed hotspots or our sampling pattern were randomly distributed throughout the survey area, we estimate the probability that a hotspot was completely missed. For each surface water measurement, the probability (P) that a hotspot was missed is calculated as a function of the total integrated hotspot area (A_h) and the total survey area (A; 6.686 km^2) of GC185

$$P = (A - A_h)/A. \tag{11}$$

Since we sampled 71 times, the probability that the hotspot was completely missed on all 71 measurements is P^{71}. This calculation clearly shows that as the area of the hotspot increases, the probability that it was missed rapidly decreases (Figure 8). While there is an increased probability that a relatively small total integrated hotspot area was missed, this relatively small area leads to a relatively small flux from hotspots. Interestingly, even if we assume a background flux of 50 times the observed value for GC185, a total integrated hotspot area of only 1.92% of the survey area is necessary to

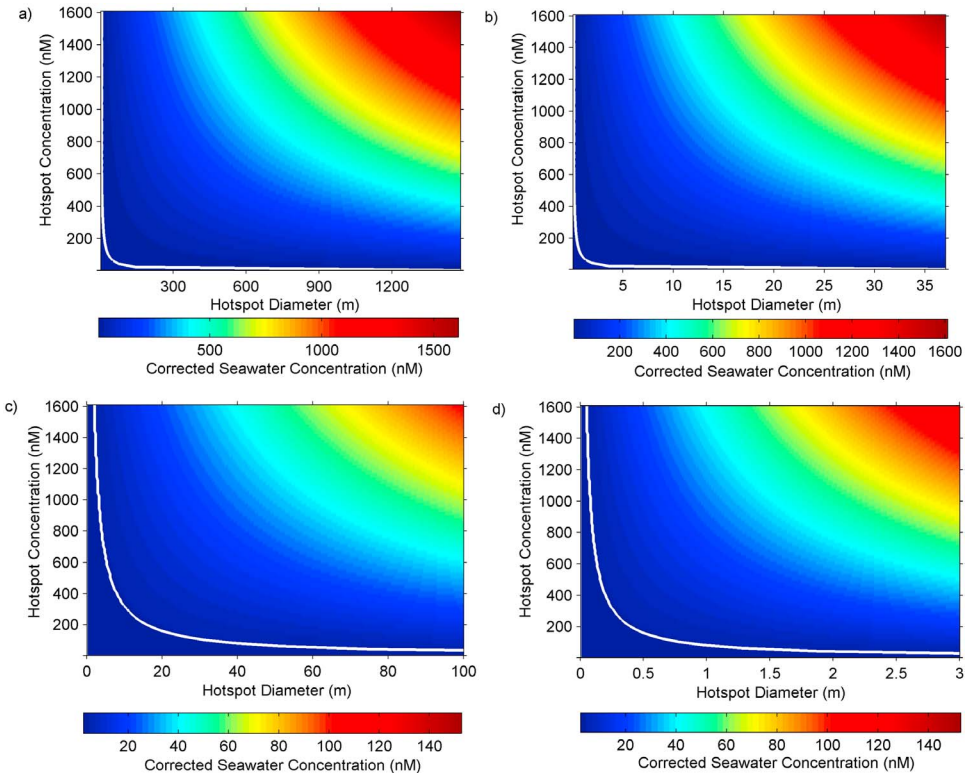

Figure 7. Corrected seawater methane concentrations (C_w) (colored contours) as a function of hotspot sizes (x-axis) and hotspot concentrations (y-axis). (a) A scenario when the ship crosses a hotspot with an infinite variety of sizes and concentrations from a background concentration of 2 nmol L^{-1} at a ship speed of 4 knots (e.g., when ship is doing coarse survey). (b) A scenario when the ship crosses a hotspot with an infinite variety of sizes and concentrations from a background concentration of 2 nmol L^{-1} at a ship speed of 0.1 knots (e.g. when ship is holding station). (c) An expansion of Figure 7a and (d) an expansion of Figure 7b are also shown. White lines indicate 4 nmol L^{-1} contours, our defined boundary for an observable hotspot signal (see section 4.4). Any concentration or size condition to the right and above the white line meets the criteria for being a detectable hotspot.

produce a daily flux similar to our "background" observations. And for a hotspot area of 1.92%, there is only a 25% chance that hotspots covering this total integrated area were missed during our sampling campaign.

5. Conclusions

[28] Elevated methane concentrations in surface seawater were observed, and elevated net sea-to-air methane fluxes were determined at three seep sites (MC118, GC 600 and GC185) in the northern Gulf of Mexico. The net sea-to-air methane fluxes ranged from −4.19 to 86.1 μmol m^{-2} d^{-1} over the deepwater hydrocarbon plume areas, agreeing with most previous studies. Variations in the atmospheric methane concentrations suggest the need for measuring atmospheric methane concentration when assessing the net sea-to-air fluxes. High temporal and spatial variability in the

Table 4. The Integrated Net Mass Flux of Methane From Each Survey Area Each Day and the Total Potential Mass Flux From Hotspots at Those Sites

Sites	Survey Area (km^2)	Mass Flux[a] (mol d^{-1})	Total Hotspot Area (km^2)	Hotspots Mass Flux[b] (mol d^{-1})
MC118				
YD 187	15.15	300	0.930×10^{-3}	5.16
YD 188	16.27	215	0.238×10^{-3}	1.34
YD 189	34.64	271	0.444×10^{-3}	1.82
YD 190	8.53	66.1	0.181×10^{-3}	0.82
YD 192.5–193.5	0.062	0.74	0.597×10^{-3}	4.66
YD 193.5–195.2	0.53	3.71	0.181×10^{-3}	0.80
Mean		142		2.43
GC600	8.57	51.9	0.051×10^{-3}	0.24
GC185	6.69	6.85	0.020×10^{-3}	0.05

[a]Integrated mass flux using natural neighbor.
[b]The total methane flux from hotspots assuming relatively small areas of hotspots exist on the survey tracks.

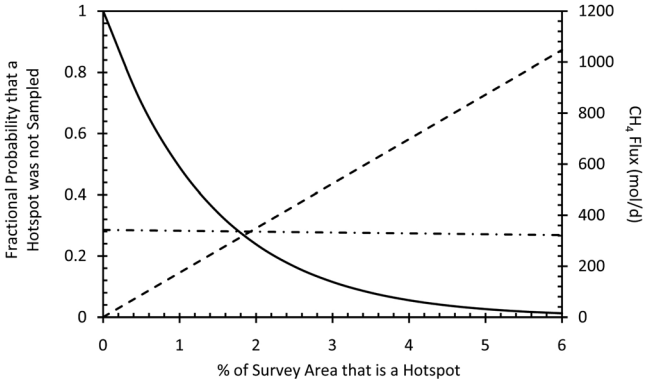

Figure 8. Hotspots potentially missed between sampled locations at GC185 as a function of assumed total hotspot area. Probability that a hotspot was missed during the survey (n = 71) (solid line). CH_4 flux from the total integrated hotspot area (dashed line). CH_4 flux from 50 times the background (i.e., nonhotspot) area at GC185 (dashed-dotted line).

methane fluxes was observed over the three seep areas. Extrapolating the highest flux from this study to other deepwater hydrocarbon seeps in the northern Gulf of Mexico suggests that diffusive net sea-to-air fluxes from deepwater hydrocarbon seeps in the northern Gulf of Mexico is an insignificant source to atmospheric methane. However, the elevated air concentrations on GC600 require about 3×10^5 mol d^{-1} of methane released in this area. This tremendous methane source could not be characterized during this study.

[29] Three orders of magnitude of discrepancy exist between the results from this study and those reported by *Solomon et al.* [2009] for the estimation of the diffusive net sea-to-air flux of methane from deepwater hydrocarbon seeps in the northern Gulf of Mexico. The large discrepancy between these two studies is mainly attributed to the different concentrations observed and the depths of those concentrations. The concentrations reported here are all from within or close to the surface mixed layer and appropriate for use in air-sea flux calculations. However, assuming that extremely high methane concentrations existed as relatively small hotspots in the surface seawater over deepwater hydrocarbon seep area, the impact of those hotspots on the regional diffusive air-sea flux would be small.

[30] **Acknowledgments.** The data reported here are available from the authors and will be submitted to the Marine Methane and Nitrous Oxide (MEMENTO) database. Information on accessing this database can be found at http://www.bodc.ac.uk/solas_integration/implementation_products/group3/. This work was supported by the Department of Energy (National Nuclear Security Administration) National Energy Technology Laboratory under Award Number DE-NT0005638. We thank TDI Brooks, the crew of R/V *Brooks McCall* and our colleagues in the HYFLUX project for all of their help. We are grateful for the constructive and helpful comments from two reviewers, especially from the reviewer one. This report was prepared as an account of work sponsored by an agency of the United States Government. Neither the United States Government nor any agency thereof, nor any of their employees, makes any warranty, express or implied, or assumes any legal liability or responsibility for the accuracy, completeness, or usefulness of any information, apparatus, product, or process disclosed, or represents that its use would not infringe privately owned rights. Reference herein to any specific commercial product, process, or service by trade name, trademark, manufacturer, or otherwise does not necessarily constitute or imply endorsement, recommendation, or favoring by the United States Government or any agency thereof. The views and opinions of authors herein do not necessarily state or reflect those of the United States Government or any agency thereof.

References

Amouroux, D., G. Roberts, S. Rapsomanikis, and M. O. Andreae (2002), Biogenic gas (CH4, N2O, DMS) emission to the atmosphere from near-shore and shelf waters of the north-western Black Sea, *Estuarine Coastal Shelf Sci.*, *54*(3), 575–587, doi:10.1006/ecss.2000.0666.

Bange, H. W., U. H. Bartell, S. Rapsomanikis, and M. O. Andreae (1994), Methane in the Baltic and North seas and a reassessment of the marine emissions of methane, *Global Biogeochem. Cycles*, *8*(4), 465–480, doi:10.1029/94GB02181.

Bange, H. W., S. Rapsomanikis, and M. O. Andreae (1996), The Aegean Sea as a source of atmospheric nitrous oxide and methane, *Mar. Chem.*, *53*(1–2), 41–49, doi:10.1016/0304-4203(96)00011-4.

Bange, H. W., S. Dahlke, R. Ramesh, L. A. Meyer-Reil, S. Rapsomanikis, and M. O. Andreae (1998), Seasonal study of methane and nitrous oxide in the coastal waters of the southern Baltic Sea, *Estuarine Coastal Shelf Sci.*, *47*(6), 807–817, doi:10.1006/ecss.1998.0397.

Boswell, R., and T. S. Collett (2011), Current perspectives on gas hydrate resources, *Energy Environ. Sci.*, *4*(4), 1206–1215, doi:10.1039/c0ee00203h.

Butler, J. H., D. B. King, J. M. Lobert, S. A. Montzka, S. A. Yvon-Lewis, B. D. Hall, N. J. Warwick, D. J. Mondeel, M. Aydin, and J. W. Elkins (2007), Oceanic distributions and emissions of short-lived halocarbons, *Global Biogeochem. Cycles*, *21*, GB1023, doi:10.1029/2006GB002732.

Clark, J. F., I. Leifer, L. Washburn, and B. P. Luyendyk (2003), Compositional changes in natural gas bubble plumes: observations from the Coal Oil Point marine hydrocarbon seep field, *Geo Mar. Lett.*, *23*, 187–193, doi:10.1007/s00367-003-0137-y.

Clark, J. F., L. Washburn, and K. Schwager Emery (2010), Variability of gas composition and flux intensity in natural marine hydrocarbon seeps, *Geo Mar. Lett.*, *30*(3–4), 379–388, doi:10.1007/s00367-009-0167-1.

Cynar, F. J., and A. A. Yayanos (1991), Enrichment and characterization of a methanogenic bacterium from the oxic upper layer of the ocean, *Curr. Microbiol.*, *23*(2), 89–96, doi:10.1007/BF02092256.

de Angelis, M. A., and C. Lee (1994), Methane production during zooplankton grazing on marine-phytoplankton, *Limnol. Oceanogr.*, *39*(6), 1298–1308, doi:10.4319/lo.1994.39.6.1298.

Denman, K. L., et al. (2007), Couplings between changes in the climate system an biogeochemistry, in *Climate Change 2007: The Physical Science Basis: Working Group I Contribution to the Fourth Assessment Report of the IPCC*, edited by S. Solomon et al., chap. 7, pp. 499–587, Cambridge Univ. Press, New York.

Frye, M. (2008), Preliminary evaluation of in-place gas hydrate resources: Gulf of Mexico outer continental shelf, *OCS Rep. MMS 2008-004*, Resour. Eval. Div., Miner. Manage. Serv., U.S. Dep. of the Inter., Washington, D. C. [Available at http://www.boemre.gov/revaldiv/GasHydrateFiles/MMS2008-004.pdf.]

Garcia-Pineda, O., I. MacDonald, B. Zimmer, B. Shedd, and H. Roberts (2010), Remote-sensing evaluation of geophysical anomaly sites in the outer continental slope, northern Gulf of Mexico, *Deep Sea Res., Part II*, *57*, 1859–1869, doi:10.1016/j.dsr2.2010.05.005.

Greinert, J., Y. Artemov, V. Egorov, M. De Batist, and D. McGinnis (2006), 1300-m-high rising bubbles from mud volcanoes at 2080 m in the Black Sea: Hydroacoustic characteristics and temporal variability, *Earth Planet. Sci. Lett.*, *244*(1–2), 1–15, doi:10.1016/j.epsl.2006.02.011.

Hornafius, J. S., D. Quigley, and B. P. Luyendyk (1999), The world's most spectacular marine hydrocarbon seeps (Coal Oil Point, Santa Barbara Channel, California): Quantification of emissions, *J. Geophys. Res.*, *104*(C9), 20,703–20,711, doi:10.1029/1999JC900148.

Hu, L., S. A. Yvon-Lewis, Y. Liu, J. E. Salisbury, and J. E. O'Hern (2010), Coastal emissions of methyl bromide and methyl chloride along the eastern Gulf of Mexico and the east coast of the United States, *Global Biogeochem. Cycles*, *24*, GB1007, doi:10.1029/2009GB003514.

Intergovernmental Panel on Climate Change (2001), *Climate Change 2001: The Scientific Basis: Contribution of Working Group I to the Third Assessment Report of the IPCC*, edited by J. T. Houghton et al., 881 pp., Cambridge Univ. Press, New York.

Johnson, J. E. (1999), Evaluation of a seawater equilibrator for shipboard analysis of dissolved oceanic trace gases, *Anal. Chim. Acta*, *395*(1–2), 119–132, doi:10.1016/S0003-2670(99)00361-X.

Kessler, J. D., W. S. Reeburgh, J. Southon, R. Seifert, W. Michaelis, and S. C. Tyler (2006), Basin-wide estimates of the input of methane from seeps and clathrates to the Black Sea, *Earth Planet. Sci. Lett.*, *243*(3–4), 366–375, doi:10.1016/j.epsl.2006.01.006.

Kourtidis, K., I. Kioutsioukis, D. F. McGinnis, and S. Rapsomanikis (2006), Effects of methane outgassing on the Black Sea atmosphere, *Atmos. Chem. Phys.*, *6*, 5173–5182, doi:10.5194/acp-6-5173-2006.

Large, W. G., and S. Pond (1982), Sensible and latent heat flux measurements over the ocean, *J. Phys. Oceanogr.*, *12*, 464–482, doi:10.1175/1520-0485(1982)012<0464:SALHFM>2.0.CO;2.

Leifer, I., and J. Boles (2005), Measurement of marine hydrocarbon seep flow through fractured rock and unconsolidated sediment, *Mar. Pet. Geol.*, *22*(4), 551–568, doi:10.1016/j.marpetgeo.2004.10.026.

Leifer, I., and I. MacDonald (2003), Dynamics of the gas flux from shallow gas hydrate deposits: Interaction between oily hydrate bubbles and the oceanic environment, *Earth Planet. Sci. Lett.*, *210*(3–4), 411–424, doi:10.1016/S0012-821X(03)00173-0.

Leifer, I., B. P. Luyendyk, J. Boles, and J. F. Clark (2006), Natural marine seepage blowout: Contribution to atmospheric methane, *Global Biogeochem. Cycles*, *20*, GB3008, doi:10.1029/2005GB002668.

Liss, P. S., and L. Merlivat (1986), Air-sea gas exchange rates: Introduction and synthesis, in *The Role of Air-Sea Exchange in Geochemical Cycling*, edited by P. Buat-Menard, pp. 113–127, Springer, New York.

Mau, S., D. L. Valentine, J. F. Clark, J. Reed, R. Camilli, and L. Washburn (2007), Dissolved methane distributions and air-sea flux in the plume of a massive seep field, Coal Oil Point, California, *Geophys. Res. Lett.*, *34*, L22603, doi:10.1029/2007GL031344.

McGinnis, D. F., J. Greinert, Y. Artemov, S. E. Beaubien, and A. Wüest (2006), Fate of rising methane bubbles in stratified waters: How much methane reaches the atmosphere?, *J. Geophys. Res.*, *111*, C09007, doi:10.1029/2005JC003183.

Nightingale, P. D., P. S. Liss, and P. Schlosser (2000), Measurements of air-sea gas transfer during an open ocean algal bloom, *Geophys. Res. Lett.*, *27*, 2117–2120, doi:10.1029/2000GL011541.

Quigley, D. C., J. Scott Hornafius, B. P. Luyendyk, R. D. Francis, J. Clark, and L. Washburn (1999), Decrease in natural marine hydrocarbon seepage near Coal Oil Point, California, associated with offshore oil production, *Geology*, *27*(11), 1047–1050, doi:10.1130/0091-7613(1999)027<1047:DINMHS>2.3.CO;2.

Ramaswamy, V., O. Boucher, J. Haigh, D. Hauglustaine, J. Haywood, G. Myhre, T. Nakajima, G. Shi, and S. Solomon (2001), Radiative forcing of climate change, in *Climate Change 2001: The Scientific Basis: Contribution of Working Group to the Third Assessment Report of the IPCC*, edited by J. T. Houghton et al., pp. 349–416, Cambridge Univ. Press, New York.

Reeburgh, W. S. (2007), Oceanic methane biogeochemistry, *Chem. Rev.*, *107*, 486–513, doi:10.1021/cr050362v.

Reeburgh, W. S., B. B. Ward, S. C. Whalen, K. A. Sandbeck, K. A. Kilpatrick, and L. J. Kerkhof (1991), Black Sea methane geochemistry, *Deep Sea Res., Part A*, *38*, S1189–S1210, doi:10.1016/S0198-0149(10)80030-5.

Reeburgh, W. S., S. C. Tyler, and J. Carroll (2006), Stable carbon and hydrogen isotope measurements on Black Sea water-column methane, *Deep Sea Res., Part II*, *53*(17–19), 1893–1900, doi:10.1016/j.dsr2.2006.03.018.

Rehder, G., P. W. Brewer, E. T. Peltzer, and G. Friederich (2002), Enhanced lifetime of methane bubble streams within the deep ocean, *Geophys. Res. Lett.*, *29*(15), 1731, doi:10.1029/2001GL013966.

Rehder, G., I. Leifer, P. G. Brewer, G. Friederich, and E. T. Peltzer (2009), Controls on methane bubble dissolution inside and outside the hydrate stability field from open ocean field experiments and numerical modeling, *Mar. Chem.*, *114*(1–2), 19–30, doi:10.1016/j.marchem.2009.03.004.

Rhee, T. S., A. J. Kettle, and M. O. Andreae (2009), Methane and nitrous oxide emissions from the ocean: A reassessment using basin-wide observations in the Atlantic, *J. Geophys. Res.*, *114*, D12304, doi:10.1029/2008JD011662.

Schmale, O., J. Greinert, and G. Rehder (2005), Methane emission from high-intensity marine gas seeps in the Black Sea into the atmosphere, *Geophys. Res. Lett.*, *32*, L07609, doi:10.1029/2004GL021138.

Solomon, E. A., M. Kastner, I. R. MacDonald, and I. Leifer (2009), Considerable methane fluxes to the atmosphere from hydrocarbon seeps in the Gulf of Mexico, *Nat. Geosci.*, *2*(8), 561–565, doi:10.1038/ngeo574.

Sweeney, C., E. Gloor, A. R. Jacobson, R. M. Key, G. McKinley, J. L. Sarmiento, and R. Wanninkhof (2007), Constraining global air-sea gas exchange for CO_2 with recent bomb ^{14}C measurements, *Global Biogeochem. Cycles*, *21*, GB2015, doi:10.1029/2006GB002784.

Takahashi, T., et al. (2009), Climatological mean and decadal change in surface ocean pCO_2, and net sea-air CO_2 flux over the global oceans, *Deep Sea Res., Part II*, *56*(8–10), 554–577, doi:10.1016/j.dsr2.2008.12.009.

Tans, P. P., I. Y. Fung, and T. Takahashi (1990), Observational constraints on the global atmospheric CO_2 budget, *Science*, *247*, 1431–1438, doi:10.1126/science.247.4949.1431.

Tilbrook, B. D., and D. M. Karl (1995), Methane sources, distributions and sinks from California coastal waters to the oligotrophic North Pacific Gyre, *Mar. Chem.*, *49*(1), 51–64, doi:10.1016/0304-4203(94)00058-L.

Wanninkhof, R. (1992), Relationship between wind speed and gas exchange over the ocean, *J. Geophys. Res.*, *97*(C5), 7373–7382, doi:10.1029/92JC00188.

Yoshida, O., H. Y. Inoue, S. Watanabe, S. Noriki, and M. Wakatsuchi (2004), Methane in the western part of the Sea of Okhotsk in 1998–2000, *J. Geophys. Res.*, *109*, C09S12, doi:10.1029/2003JC001910.

Yvon-Lewis, S. A., L. Hu, and J. Kessler (2011), Methane flux to the atmosphere from the Deepwater Horizon oil disaster, *Geophys. Res. Lett.*, *38*, L01602, doi:10.1029/2010GL045928.

L. Hu, J. D. Kessler, and S. A. Yvon-Lewis, Department of Oceanography, Texas A&M University, 3146 TAMU, College Station, TX 77843, USA. (leihu@tamu.edu)

I. R. MacDonald, Earth Ocean Atmosphere Department, Florida State University, 117 N Woodward Dr., PO Box 3064320, Tallahassee, FL 32306, USA.